
Statistical Testing for Efficient Out of Distribution Detection in Deep Neural Networks

Matan Haroush^{*12} Tzviel Frostig^{*3} Ruth Heller³ Daniel Soudry²

Abstract

Commonly, Deep Neural Networks (DNNs) generalize well on samples drawn from a distribution similar to that of the training set. However, DNNs' predictions are brittle and unreliable when the test samples are drawn from a dissimilar distribution. This presents a major concern for deployment in real-world applications, where such behavior may come at a great cost — as in the case of autonomous vehicles or healthcare applications.

This paper frames the Out Of Distribution (OOD) detection problem in DNN as a statistical hypothesis testing problem. Unlike previous OOD detection heuristics, our framework is guaranteed to maintain the false positive rate (detecting OOD as in-distribution) for test data. We build on this framework to suggest a novel OOD procedure based on low-order statistics. Our method achieves comparable or better than state-of-the-art results on well-accepted OOD benchmarks without retraining the network parameters — and at a fraction of the computational cost.

1. Introduction

Deep Neural Networks' (DNNs) predictions were shown to be overconfident and unreliable when the test samples are drawn from an unexpected distribution (Biggio et al., 2013; Szegedy et al., 2013; Goodfellow et al., 2014; Eykholt et al., 2017). This issue can be seen as a problem of uncertainty modeling, which can be applied for Out of Distribution (OOD) detection. Uncertainty modeling has been extensively studied over the past several decades (Hellman, 1970; Bridle, 1990; MacKay, 1992; Cordella et al., 1995; Schölkopf et al., 2000; Papadopoulos, 2008). Contemporary methods for OOD detection in DNNs such as Lee et al.

(2018); Sastry & Oore (2019); Zisselman & Tamar (2020); Raghuram et al. (2020) generally assign a confidence measure to the network predictions that are used to reject the input sample if it is rated below some threshold.

However, as we explain in the next section, these methods are either computationally expensive or may lead to degraded performance (on OOD detection or the classification task). Moreover, to the best of our knowledge, they do not provide statistical guarantees for the proposed algorithms.

By treating OOD detection as a statistical hypothesis testing problem, we can design a detection procedure inspired by its vast literature — from the goodness of fit test (Pearson, 1900) to modern methods used to differentiate between multivariate distributions (e.g., Heller & Heller (2016)).

Contributions. We propose a novel framework based on statistical hypothesis testing for DNNs. Our framework quantifies how unlikely it is for a given sample to be drawn from the expected distribution by providing a p -value and maintains the false positive rate for unseen data.

Our suggested framework can be viewed as a conformal anomaly detection method, which falls under the inductive conformal predictor framework (Papadopoulos, 2008). We utilize a non-conformity measure, estimate its distribution on an in-distribution validation, and use the distribution to test if a sample is OOD. We generalize the scope of this framework by applying the non-conformity measure across the entire network. In addition, we show empirically that this generalization is crucial for OOD detection (Section 5.2).

In addition, we design a highly efficient and accurate detection scheme within our proposed framework, denoted as MaSF (Max-Simes-Fisher), that is appealing for real-world applications within a limited compute budget. Moreover, we demonstrate potential avenues to further reduce the computational overhead via structured sparsity (i.e., channel sampling) with marginal test power loss.

2. Related Work

In the context of (non-Bayesian) DNNs, previous methods for OOD detection can be roughly divided into two classes.

^{*}Equal contribution ¹Habana Labs Research. Caesarea, Israel
²Department of Electrical Engineering. Technion, Haifa, Israel
³Department of Statistics. Tel Aviv University, Tel Aviv, Israel.
 Correspondence to: Matan Haroush <mharoush@habana.ai>, Tzviel Frostig <tfrostig@gmail.com>.

”Mutators” methods modify the network structure and/or depend on training its parameters to provide a confidence measure (Blundell et al., 2015; Hendrycks et al., 2018; Malinin & Gales, 2018; Winkens et al., 2020; Zhang et al., 2020; Hsu et al., 2020).

”Observer” methods model the prediction uncertainty of a pre-trained network, without modifying its architecture or parameters (Hendrycks & Gimpel, 2016; Geifman & El-Yaniv, 2017; Liang et al., 2017; Lee et al., 2018; Zisselman & Tamar, 2020; Raghuram et al., 2020).

Mutator methods are potentially costly, as they require substituting or retraining the network and subsequently repeating an exhaustive hyperparameter tuning process. Also, the resulting model quality on the original task may vary. Finally, to the best of our knowledge, such methods have no guarantees on the OOD detector’s statistical properties. Alternatively, observer methods commonly utilize auxiliary models to monitor features produced by the reference network. Since this approach is decoupled from the network optimization process, the reference accuracy is retained at the cost of additional test time resources such as compute and memory.

Another differentiating factor between methods, regardless of their class, stems from fundamental assumptions regarding prior knowledge on the test distribution. Specifically, some methods (e.g., Hendrycks et al. (2018); Lee et al. (2018); Zisselman & Tamar (2020)) rely on prior knowledge, such as access to the OOD data or its proxy. However, this can lead to undesirable bias and poor detection performance on unknown test distributions.

Since our proposed framework does not rely on modifying the model or its parameters, we will focus on reviewing the relevant observer methods and related work.

Hendrycks & Gimpel (2016) proposed using raw Softmax (Bridle, 1990) scores as a baseline method for OOD detection, positioned on the observation that a well-trained DNN tends to assign a higher probability to in-distribution vs. OOD examples. Liang et al. (2017) presented ODIN as an improvement to the baseline method by combining Softmax temperature scaling with a costly input pre-processing strategy. The temperature and perturbations magnitude hyperparameters are calibrated on OOD samples.

Lee et al. (2018) and Quintanilha et al. (2018), utilized additional layers of the network for OOD detection. Quintanilha et al. (2018) suggested training logistic regression on the per-layer average mean and variance using OOD datasets. Alternatively, Lee et al. (2018) suggested employing the Mahalanobis distance over per-channel mean values under a Linear Discriminant Analysis (LDA) assumption (i.e., the covariance matrix is not class-dependent). The method selects the minimal values per-class & layer, then combines

them using logistic regression on a small subset of the OOD dataset. The authors suggested replacing OOD data with adversarial examples as a proxy with diminished results. Zisselman & Tamar (2020) extends this idea by replacing the Mahalanobis distance with a learned likelihood function, using deep residual-flow models. Similarly to Lee et al. (2018), the method leverages the aforementioned pre-processing strategy in conjunction with the residual-flow model, while scores are combined using logistic regression following the same procedures.

A parallel line of work inspired by Lee et al. (2018) includes Sastry & Oore (2019) and Yu et al. (2020). Sastry & Oore (2019) suggested an alternative score based on the outer product over intermediate feature maps (Gram matrix). The authors consider the total deviation from the minimal and maximal values observed on the training data for several Gram matrix exponent orders. Each layer’s contribution to the total sum is normalized by the mean deviation over a portion of the validation set.

Yu et al. (2020) proposed MALCOM, where the feature summary function is based on the Normalized Compression Distance (NCD), aimed to capture spatial patterns missed by average pooling employed by other methods. Unlike Lee et al. (2018), the authors avoid using OOD data by computing a single Mahalanobis distance on the flattened NCD values from all layers. This approach will lose its detection accuracy when the training set size is small compared to the number of parameters required for estimation (i.e., the covariance matrix and mean vector of all layers).

To the best of our knowledge, Grosse et al. (2017) were the first to adopt a statistical hypothesis test to detect adversarial examples in DNNs. The method is based on the Maximum Mean Discrepancy (MMD) test for equality of distributions between two groups. The test statistic distribution is estimated using permutations (i.e., shuffling the labels of the two compared groups). The method can only be used on groups with a significant number of OOD samples. Hence, it cannot be used to flag a single observation as OOD. Moreover, it is extremely computationally expensive.

Recently, Raghuram et al. (2020) also suggested an approach based on statistical hypothesis testing at each layer for detecting adversarial attacks. The suggested test statistics are based on K-Nearest Neighbours (K-NN), where the neighborhood is determined based on the Euclidean distance between flattened feature maps. The obtained p-values are then combined using classical p-values combinations tests. However, the procedure’s final output is not a valid p-value, as the dependency between the combined p-values is ignored. Thus, the assumption regarding the combination test statistic distribution does not hold (see Section-3.1). Moreover, this approach has two crucial drawbacks: First, K-NN requires computing the per-layers’ features distance

between the test sample and the entire training dataset. Second, due to the use of flattened feature maps, this method suffers from the phenomenon known as "the curse of dimensionality" when used in conjunction with large inputs. We associate these flaws with the method's relatively low detection scores on simple OOD benchmarks compared to Lee et al. (2018) baseline.

3. Statistical testing background

In the following section, we provide a brief summary for Null Hypothesis Statistical Testing (NHST). We begin with a single hypothesis and then explain the various methods of testing multiple hypotheses. In Section 4 we present how they are used in our proposed framework for DNNs.

NHST is the process of choosing between two hypotheses - \mathcal{H}_0 (null) and \mathcal{H}_1 (alternative) regarding observation (sample) X . It is formalized as $\mathcal{H}_0 : X \sim \mathcal{P}$ vs $\mathcal{H}_1 : X \not\sim \mathcal{P}$. \mathcal{P} is some distribution. For simplicity of exposition, we assumed \mathcal{P} is a single distribution, but the null hypothesis can also contain instead a family of distributions (e.g., all distributions with expectation zero).

The decision to reject \mathcal{H}_0 is based on the critical value γ and the test statistic $T(X)$. Throughout this section, we will focus on right-tailed tests. We call a test right-tailed when assuming that higher values of $T(X)$ are more likely under \mathcal{H}_1 than under \mathcal{H}_0 . In those kinds of tests, we say that \mathcal{H}_0 is rejected if $T(X) > \gamma$; otherwise, we accept it. The critical value γ quantifies the required evidence sufficient to determine if \mathcal{H}_0 is false.

Since the inference is based on random data, X , there is always a chance for a wrong decision. Erroneously rejecting \mathcal{H}_0 , is called a type I error (TIE). The significance level (i.e., probability of TIE) is given by $\alpha = P_{\mathcal{H}_0}(T(X) > \gamma)$. Usually, α is predetermined, and γ is found accordingly. For a given significance level, the goal is to maximize the power of the test, $P_{\mathcal{H}_1}(T(X) > \gamma)$, which is the probability of correctly rejecting \mathcal{H}_0 .

Commonly, a p-value is used to summarize NHST. The p-value indicates the probability of obtaining a value equal or more extreme than the observed test statistic, given that \mathcal{H}_0 is true. The p-value is given by, $q(t_{\text{obs}}) = P_{\mathcal{H}_0}(T(X) \geq t_{\text{obs}})$, where t_{obs} is the observed value of the test statistic.

Assuming the null is correct, and that \mathcal{P} is continuous, then the p-values are uniformly distributed (Abramovich & Ritov (2013) Proposition 4.1). This allows to simply reject the null if $q(t_{\text{obs}}) \leq \alpha$. It is clear that the significance level will be maintained if the p-value distribution is stochastically larger than or equal to the uniform distribution (X is stochastically smaller than Y if $\forall x : P(X > x) < P(Y > x)$).

When it is unclear if $T(X)$ is expected to be larger or smaller

under \mathcal{H}_1 , one can use two-sided tests, so the p-value is $2 \cdot \min[P_{\mathcal{H}_0}(T(X) > t_{\text{obs}}), P_{\mathcal{H}_0}(T(X) < t_{\text{obs}})]$, which can be viewed as conducting a right and left sided tests and combining the results. For non-symmetric \mathcal{P} the p-value is conservative (TIE is less than α).

3.1. Global Null Tests

In some cases, we care about a set of hypotheses and testing whether none of these hypotheses are false (the global null). Combination tests are used in such cases.

Let \mathbf{q} denote a vector of m p-values, $\mathbf{q} = (q_1, \dots, q_m)$, used to test m null-hypotheses, $H_{0,1}, \dots, H_{0,m}$. The global null hypothesis is defined as $H_{0,\cdot} = \bigcap_{i=1}^m H_{0,i}$. The test statistic is $T(\mathbf{q})$. Every combination test summarizes \mathbf{q} differently. Hence their respective powers differ, depending on the unknown distribution of the test statistic under \mathcal{H}_1 .

Why should we combine p-values rather than other summary statistics? To motivate this, we note that p-values reduce the test statistic into a scale between 0 and 1 of "unlikeliness" under the null. When aggregating tests, this feature is useful as all of the test statistics are comparable. For example, suppose we have $Y_1 \sim \chi_1^2$ and $Y_2 \sim \text{Exp}(10^{-1})$, and two respective samples from these distributions: $y_1 = 1$ and $y_2 = 15$. Which sample is more extreme, i.e., less likely? The different magnitudes of the random variables make it hard to compare the observations directly. However, examining the p-values $q_1 = 0.16$ and $q_2 = 0.22$, we find that the y_1 is a more extreme quantile of its distribution. Thus, when aggregating test statistics, it is also useful to turn them to p-values, as it ensures that all of them have an equal contribution.

Two common tests of the global-null are Fisher (Fisher, 1992) and Simes (Simes, 1986).

The Fisher combination test statistic is $T_{\text{Fisher}}(\mathbf{q}) = -2 \sum_{i=1}^m \ln(q_i)$. If the p-values are independent and have a uniform null distribution, then $T_{\text{Fisher}}(\mathbf{q}) \sim \chi_{2m}^2$ when the global null hypothesis is true. Otherwise, the null distribution of the test statistic is unknown. In the first case, the critical value of $\gamma = \chi_{2m, 1-\alpha}^2$ will ensure the TIE is maintained at the specified level α if the global null hypothesis is rejected when $T_{\text{Fisher}}(\mathbf{q}) \geq \gamma$. While in the second case, the appropriate quantile estimate can be used instead.

Simes test (Simes, 1986), involves ordering the p-values, $q_{(1)} \leq q_{(2)} \leq \dots \leq q_{(m)}$, and calculating the following test statistic $T_{\text{Simes}}(\mathbf{q}) = \min_{i \in \{1, \dots, m\}} q_{(i)} \frac{m}{i}$. If the p-values are independent and have a uniform null distribution, then $T_{\text{Simes}}(\mathbf{q}) \sim \text{Uniform}[0, 1]$ when the global null is true. Implying that rejecting the global null for T_{Simes} will maintain the TIE (Simes, 1986). When these assumptions are not met, one may use the eCDF, as with the Fisher test statistic.

To demonstrate how these tests differ from one another, consider testing if μ , the mean vector of m features, is zero. The evidence against the null (signal) is dense if the number of non-zero entries in μ is large and sparse if only a few entries in μ are non-zero (assuming μ magnitude is fixed). The Simes test is best suited to detect a sparse signal, as small p-values will dominate the value of T_{Simes} . In contrast, the Fisher combination test performs better when the signal is dense since T_{Fisher} aggregates the p-values of all features. See [Cheng & Sheng \(2017\)](#) for a simulation comparing the two methods.

4. Hypothesis testing in neural networks

For the sake of simplicity, we focus the next section solely on convolutional neural networks (CNN) for image classification tasks. The method presented, however, is applicable for any DNN.

Define $[k] = \{i \in \mathbb{N} : i \leq k\}$ and let $\chi^c = \{(X_i, y_i) : i \in [n_c], y_i = c\}$, where $|\chi^c| = n_c$, X_i is an image and y_i, \hat{y}_i are its true and predicted class (out of k classes). The measurement set is denoted by $\chi = \bigcup_{c=1}^k \chi^c$, and its cardinality is $N = \sum_{c=1}^k n_c$. We assume the data is generated from $\mathcal{P} = \{\mathcal{P}^c : c \in [k]\}$, where \mathcal{P}^c is the class distribution.

The distribution of any test statistic under \mathcal{H}_0 is required to obtain p-values. For that reason we apply the eCDF to estimate the null distribution of class c and function T at x ,

$$\hat{\mathbb{P}}(x; T, \chi^c) = \frac{\sum_{(X_i, y_i) \in \chi^c} I(T(X_i) \leq x) + 1}{n_c + 1}. \quad (1)$$

Note that observations from χ are assumed to be independent of the data used to train the weights of the network. The addition of 1 in the numerator is to ensure that we do not obtain p-values that equal 0, as it implies they are rejected at all significance level.

The problem of determining if an image X_{test} is OOD, can be formalized as

$$\mathcal{H}_0^* : \exists c : X_{\text{test}} \sim \mathcal{P}^c, \quad \mathcal{H}_1^* : X_{\text{test}} \not\sim \mathcal{P}^c \quad \forall c \in [k] \quad (2)$$

Meaning, rejecting \mathcal{H}_0^* implies that the image is unlikely to be from any of the class distributions. This definition is independent from the predicted or true class of the image. One can also test if an image is sampled from a specific class distribution,

$$\mathcal{H}_0^c : X_{\text{test}} \sim \mathcal{P}^c, \quad \mathcal{H}_1^c : X_{\text{test}} \not\sim \mathcal{P}^c. \quad (3)$$

Since the true label is unknown at test time, we are interested in the case where the class is assigned according to the CNN prediction, $\mathcal{H}_0^{\hat{y}_{\text{test}}}$. Therefore, rejecting it indicates the image is either misclassified or OOD.

Our approach's main idea is to leverage the hierarchical computation in CNN for NHST by gradually aggregating evidence against one of the above hypotheses.

4.1. Testing at individual channels

The typical CNN (F) is composed of L layers, each layer, l , contains a_l channels. The feature map of the j 'th channel in l 'th layer is denoted by $F_{j,l} : X \rightarrow \mathbb{R}^{h_l \times w_l}$, where X is the input image, h_l and w_l refer to the spatial dimensions of the feature maps at the l 'th layer. We begin by testing at the channel level.

Each channel is summarized to a scalar value using a spatial reduction function, T^S ,

$$t_{j,l}(X) = T^S(F_{j,l}(X)) \quad | \quad T^S : \mathbb{R}^{h_l \times w_l} \rightarrow \mathbb{R}. \quad (4)$$

Therefore, the empirical null distribution of the $t_{j,l}$ at channel j in layer l is $\hat{\mathbb{P}}(x; t_{j,l}, \chi^c)$. The derived p-value is denoted as $q_{j,l}^c$, and $q_{.,l}^c$ refers to the entire layer. We use two-sided p-values for the channel reduction, as outliers can appear in both tails of the distribution, see Section-D.1.

4.2. Combining test results

We now wish to aggregate the evidence from $q_{.,l}^c$ for each layer, by applying a channel reduction function, denoted by T^{ch} as follows,

$$t_l^c(X) = T_l^{\text{ch}}(q_{.,l}^c) \quad | \quad T_l^{\text{ch}} : [0, 1]^{a_l} \rightarrow \mathbb{R}. \quad (5)$$

By employing $\hat{\mathbb{P}}(x; t_l^c, \chi^c)$, we can recover the layer's p-values for class c : q_1^c, \dots, q_L^c . Given q_1^c, \dots, q_L^c for all layers, the class conditional test statistic of an image is obtained by applying the layer reduction function, T^L ,

$$t^c(X) = T^L(q_1^c, \dots, q_L^c) \quad | \quad T^L : [0, 1]^L \rightarrow \mathbb{R}. \quad (6)$$

The class conditional p-value for sample X , derived using $\hat{\mathbb{P}}(x; t^c, \chi^c)$ and denoted by $q^c(X)$, can be used for testing \mathcal{H}_0^c (Eq. 3).

We now turn to present the two main propositions regarding the validity of the procedure described above. The procedure is considered valid if it maintains the TIE at the specified significance level. Proof for both propositions can be found in the Appendix (Section-B).

Proposition 1 For testing \mathcal{H}_0^* versus \mathcal{H}_1^* , the probability of TIE is less than α , using

$$q^{\max}(X_{\text{test}}) = \max\{q^1(X_{\text{test}}), \dots, q^k(X_{\text{test}})\},$$

i.e., $P_{\mathcal{H}_0^*}(q^{\max}(X_{\text{test}}) \leq \alpha) \leq \alpha$.

Since the true class of the image is unknown, the maximum p-value ensures the method rejects the hypothesis for a sample only if it is unlikely under all classes.

When the class is assigned according to the CNN prediction (i.e., testing $\mathcal{H}_0^{\hat{y}_{\text{test}}}$), the TIE is larger than the significance level. We can bound this error as stated in the next proposition and adjust the p-values accordingly to obtain a valid test.

Proposition 2 *For testing $\mathcal{H}_0^{\hat{y}_{\text{test}}}$ versus $\mathcal{H}_1^{\hat{y}_{\text{test}}}$, the probability of TIE using $q^{\hat{y}_{\text{test}}}$ is*

$$P_{\mathcal{H}_0^{\hat{y}_{\text{test}}}}(q^{\hat{y}_{\text{test}}} \leq \alpha) \leq \alpha P(\hat{y}_{\text{test}} = y_{\text{test}}) + P(\hat{y}_{\text{test}} \neq y_{\text{test}}).$$

4.3. Summary and challenges

To summarize, our approach, introduced in this section, consists of 3 steps: (i) Spatial reduction followed by p-value extraction per channel. (ii) Channel reduction, summarizing resulting p-values for each layer. (iii) Layer reduction, aggregating p-values from all layers to a single p-value.

Transforming each channel’s spatial features into a p-value ensures that no single channel dominates the function due to its magnitude. At each layer, the aggregation of the per-channel results can cause a disparity (layers with more channels dominate). Transforming the layer test statistics into p-values resolves the issue (see Appendix Section E for further details). Ultimately, this hierarchical approach guarantees a fair comparison at each step when pooling evidence from the entire CNN to reject either \mathcal{H}_0^c or \mathcal{H}_0^* .

However, combining hypotheses tests into a single test has its challenges. On the one hand, we want to include as many hypotheses, as the rejection of the global null can be caused by any of them. On the other hand, as more true null hypotheses are included, the power decreases. We posit this as a classic trade-off between bias and variance. For example, consider the case where the combined p-values are independent under the null. In the Fisher test, the more test statistics from true null hypotheses are combined, the greater the variance. This implies that the rejection criteria will be harder to reach. In the Simes test, the sorted p-values are multiplied by the number of hypotheses, m . Again, implying that adding test statistics from true null hypotheses will lower the power of the test.

5. Designing test statistics for OOD detection

So far, we have described our novel theoretical framework for NHST in DNNs. Before we proceed to describe our proposed OOD detection algorithm, we briefly review a popular benchmark used to evaluate it, and motivate the rationale behind the specific design choices we made.

5.1. OOD detection benchmark

When comparing the various OOD methods, we adhere to the same evaluation protocol from Lee et al. (2018), com-

monly used for comparability. We use the same pre-trained image classification CNNs (Huang et al., 2016; He et al., 2016) and datasets. In this benchmark, samples drawn from alternative datasets are presented to the reference CNN, while competing methods output an OOD score based solely on the CNN’s induced feature maps. Results are reported for each OOD dataset as the correct OOD predictions rate (i.e., True Positive Rate — TPR) while maintaining a False Positive Rate (FPR) of 5% for in-distribution validation samples (i.e., TPR95). This means that unlike classical NHST, the rejection threshold for the predicted OOD score is determined based on the in-distribution test set.

To accommodate this popular benchmark, we modify our procedure accordingly. First, we estimate the percentiles of the null distributions using the CNN training set. Second, we set the rejection threshold based on the validation set instead of a fixed significance level (α). This violates the statistical guarantees of maintaining TIE due to the dependency between the CNN weights and the training set samples. However, as we show later, our method empirically works well in most cases, even in this challenging setting. Additionally, since demonstrating the procedure’s ability to maintain TIE is of independent interest, we provide additional simulations employing a hold-out set in the Appendix (Section-B.2).

Finally, we wish to avoid drawing conclusions based on individual DNN and test data (i.e., scenario) results. Thus, we consider the overall performance of the evaluated method. Namely, we argue that since OOD detectors’ performance may vary greatly between scenarios (see Section-5.3) and unless the real-world and test scenarios are aligned, it is reasonable to favor an algorithm based on its relative consistency across all scenarios within the target benchmark. Therefore, to evaluate the overall performance, we calculate the mean TPR95 (mTPR) and standard deviation (SD), along with the minimal TPR95 observed — as commonly practiced in other multi-scenario domains.

5.2. Design considerations

We now turn to discuss our OOD algorithm, which returns a class conditional p-value (i.e., Hypothesis \mathcal{H}_0^c from Eq. 3) provided the trained network, input image, and class of interest.

Constructing eCDFs. Since the interest lies in small p-values (implying an OOD sample), we focus the eCDF estimation on the channel distribution tails. In practice, we estimate a fixed set of tail percentiles for the spatial reductions. This also reduces the memory footprint of the algorithm.

Choosing reductions. The choice of reduction functions can greatly impact the power of the final test statistic. Fur-

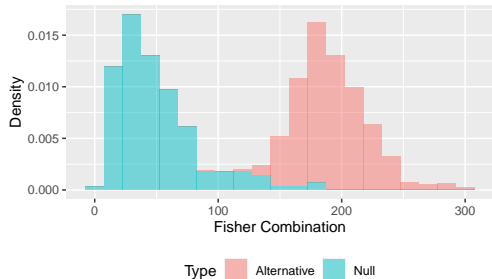


Figure 1. The empirical distribution of the class conditional MaSF test statistic for digit “0” from the SVHN dataset (blue). The alternative distribution is based on the remaining digits.

therefore, they can incorporate domain knowledge into the designed detector. We construct a set of detectors employing Simes and Fisher tests as the channel or the layer reductions along with Max and Mean pooling as spatial reductions. In Table-1 we evaluate the mean and SD of each configuration (see Section-5.1) and sort them according to mTPR. As expected, the maximum value of a given feature map is more sensitive to outliers compared to the mean value.

Additionally, the Fisher combination test performs best as a layer reduction, despite the dependency between layers (which contributes to the final statistic’s variance). This suggests the evidence of abnormality tends to propagate throughout the network, which is unlikely for in-distribution examples. Finally, the Simes test is a better channel reduction. This suggests that OOD evidence is either sparse (i.e., abnormality exists in a few of the channels) or that channels are strongly correlated, rendering the Fisher test uninformative.

Moving forward, we focus on the best configuration: Maximum (spatial), Simes (channel), and Fisher (layer) configuration, dubbed MaSF (Max-Simes-Fisher). Fig. 1 depicts an example of the empirical null and alternative distribution using this configuration.

Layer	Channel	Spatial	mTPR [†]	SD
Fisher	Simes	Max	96.1	4.4
Fisher	Fisher	Max	92.5	8.5
Fisher	Simes	Mean	89.7	9.5
Simes	Fisher	Max	88.5	11.3
Fisher	Fisher	Mean	85.7	12.6
Simes	Fisher	Mean	77.3	15.7
Simes	Simes	Max	47.7	38.3
Simes	Simes	Mean	42.0	29.0

Table 1. Comparing alternative hierarchical reduction schemes. Results are sorted according to the mean TPR95 on OOD benchmark (Section-5.1). We also report mTPR standard deviation. MaSF (Max-Simes-Fisher) outperforms all others schemes by a significant margin.

Observing multiple layers. We aim to understand the benefit of utilizing multiple layers compared to single layers. Therefore, we evaluate mTPR when using only a single layer from the end of the reference model. The MaSF detector, in this case, is naturally reduced to MaS by eliminating the Fisher layer reduction step. We consider using the inputs or outputs of the linear classifier and the penultimate layer’s inputs (i.e., the final Average Pooling layer). Observing the penultimate layer’s input achieved the best results in terms of mTPR (SD) of 64.7 (21.5). However, these are significantly lower compared to 96.1 (4.4) when tracking all layers. Thus, we conclude that the additional layers contain useful information that can be leveraged to improve OOD detection compared to monitoring a single layer from the end of the model.

Despite the potential gains from observing additional deep layers, the test power could decrease when adding non-informative layers (see Section-4.3), and the computational cost increases. We further note that the choice of which layers to test is not trivial. It may vary depending on the network architecture, downstream task, or computational budget. Thus, in our experiments, we simply test the outputs of all convolution and dense layers in the network. In the Appendix (Section-D), we provide additional analysis on the correlation between the test statistics among the monitored layers. We suggest that variance reduction techniques should play a role in the design of new algorithms within our framework. For example, introducing random sampling or grouping strategies into the construction of the test statistics, we defer this topic for future work.

5.3. Main empirical results

In this section, we breakdown MaSF performance on the popular benchmark described in Section-5.1. We compare our results with methods that followed the same benchmark rules and do not rely on retraining the model (i.e., observer methods). These methods are Deep Mahalanobis (Lee et al., 2018), ResFlow (Zisselman & Tamar, 2020) and GRAM (Sastry & Oore, 2019). To provide a fair evaluation, we disregard results tuned on OOD data. We suggest it is simple to integrate such knowledge within our framework by selecting which layers and channels to monitor, based on their discriminative power versus the test distribution. Additionally, we defer common Area Under Receiver Operating Characteristics (AUROC) to the Appendix (Section-F.3). We suggest AUROC is not well suited for OOD detection since it equally weighs TPR for all FPR, while lower T1E rates are predominantly more relevant in practical applications.

We present a summary of the results in Table-2. Despite its simplicity, the MaSF statistic outperforms other methods with respect to the mTPR, SD, and Min-TPR metrics. MaSF detection quality is consistent across models and datasets,

while other methods that perform extremely well on several benchmarks fail on others. This is reflected by the worst TPR95 observed for each method.

In particular, CIFAR-100 (as in-dist) appears to be challenging for Mahalanobis and ResFlow. We conjecture that the small dataset size leads to a loss of performance since these methods involve estimating and inverting large covariance matrices. This is a known phenomenon. For instance, Bai & Saranadasa (1996) showed a decrease in the Hotelling test’s power as the number of observations approach the number of dimensions. In contrast, GRAM and MaSF maintain their respected performance despite the limited number of samples, as they do require estimating fewer parameters.

GRAM and MaSF yield comparable TPR95 results, while MaSF has a clear advantage considering mTPR and TPR95 of the worst scenario. Surprisingly, GRAM does not improve on SVHN when compared to CIFAR-100 (as in-distributions), indicating that it may not benefit from a significantly larger training set. We provide additional results and analysis for adopting Deep Mahalanobis and GRAM into our framework in Appendix-F.

5.4. Evaluation of computational cost

Computational cost is a key element when choosing an algorithm for a specific application. This was often overlooked by prior work. Direct comparison of the computational cost for different methods may not be trivial due to the fundamental differences between procedures and the potential for optimizing specific implementations. Thus, we suggest measuring the Test statistic Computation Time (TCT) to approximate the cost of similar methods that use a form of summarizing functions over intermediate feature maps.

We propose a simple benchmark, measuring the mean execution time of the test statistic (mTCT) and the mean global TCT time over all convolution layers in MobileNet-V2 (Sandler et al., 2019). This choice is arbitrary. However, it serves as a typical DNN intended for edge devices, where resources are limited. In addition, we report the network compute time (measured independently from TCT) as a reference. Moreover, test time optimizations are not used (e.g., reduced precision, operator fusion, etc.). Hence, in real scenarios, the network’s compute time can be reduced significantly, and TCT is expected to become even more dominant. The full settings for this benchmark are in the Appendix (Section-C).

Results in Table-3 include Mahalanobis distance (under LDA assumption) as a popular baseline, GRAM deviation score as the lead competitor, and our proposed method (MaSF). We note that Mahalanobis’ TCT in this table reflects a significantly lower cost compared to the full procedure from Lee et al. (2018) since it does not include the

costly input pre-processing strategy. This strategy involves introducing perturbations to the input features at test time to increase their likelihood under the predicted class via backpropagation and a forward pass. When just using a single forward pass, as in Tabel-3, Mahalanobis’ detection quality is significantly reduced, compared to the full method results (as reported in Table-2).

Finally, MaSF mTCT is smaller by a factor of x35 and x2.5 when compared to the GRAM and the Mahalanobis (without input pre-processing) statistics. Moreover, the MaSF statistic does not involve general matrix-matrix multiplication. Hence, the computation of the MaSF statistic can run concurrently on appropriate hardware without blocking resources that are also required for the CNN inference. Therefore, the compute conditions used to produce Table-3 are in favor of the alternative methods, and the observed speedup of MaSF is expected to increase on small devices.

5.5. Random channels selection

A popular trend in DNN design favors large models, where the number of parameters is greater than the number of available training samples. Naturally, the number of estimated parameters in the OOD detector is likely to increase as well. This presents a challenge from two aspects. First, from the statistical efficiency perspective, more samples are required to achieve the same power. Second, it leads to an additional computational burden.

This section explores dimensionality reduction via random channel selection and focuses on a simple scenario where a subset of channels is randomly selected for each layer. These subsets remain fixed during the measurement and evaluation phases of the test statistics. Table-4 presents the mTPR of the MaSF variants on the same benchmark as in Table-2, where the channels are sampled uniformly for each layer, reducing the total number of channels by a given rate. Results are averaged over five random seeds.

Surprisingly, the MaSF statistic’s power is not dramatically affected by the proportion of channels, indicating that the OOD signal is present across all channels. This implies that in some cases, channel sampling can be used to decrease the method test-time cost. In this case, MaSF suffers from negligible degradation (< 1%) while using only 10% of the total number of channels, theoretically reducing the TCT cost by x10. We present additional sampling experiments in the Appendix Section-F.

6. Discussion

This paper frames the OOD detection task as a statistical hypothesis testing problem and presents a novel statistical testing framework for DNNs. Our approach quantifies the unlikelihood of a sample compared to the in-distribution data

Statistical Testing for Efficient Out of Distribution Detection in Deep Neural Networks

Network	In-dist	Out-of-dist	Mahalanobis	ResFlow	GRAM	MaSF (ours)
DenseNet	CIFAR-10	SVHN	89.6	86.1	96.1	98.6
		TinyImageNet	94.9	96.1	98.8	97.9
		LSUN	97.2	98.1	99.5	99.2
	CIFAR-100	SVHN	62.2	48.9	89.3	89.0
		TinyImageNet	87.2	91.5	95.7	93.4
		LSUN	91.4	95.8	97.2	96.5
	SVHN	CIFAR-10	97.5	90.0	80.4	88.4
		TinyImageNet	99.9	99.9	99.1	99.8
		LSUN	100	100.0	99.5	100.0
ResNet	CIFAR-10	SVHN	75.8	91.0	97.6	98.9
		TinyImageNet	95.5	98.0	98.7	98.1
		LSUN	98.1	99.1	99.6	99.5
	CIFAR-100	SVHN	41.9	74.1	80.8	86.2
		TinyImageNet	70.3	77.5	94.8	92.7
		LSUN	56.6	70.4	96.6	94.5
	SVHN	CIFAR-10	94.1	96.6	85.8	98.0
		TinyImageNet	99.2	99.9	99.3	99.9
		LSUN	99.9	100.0	99.6	100.0
mTPR			86.1	89.6	94.9	96.1
SD			17.4	13.8	6.4	4.4
Min-TPR95			41.9	48.9	80.4	86.2

Table 2. TPR95 of competing OOD detectors on a popular benchmark (Section-5.1). Our method (MaSF) performance is comparable or better to SOTA in individual tests while beating SOTA on mTPR, SD, and the worst TPR95 while being significantly more efficient (Table-3). Results for Mahalanobis and ResFlow reflect detection accuracy when tuned using adversarial examples and include input pre-processing.

Method \ TCT	Single (ms)		Total (ms)		Relative
	Mean	SD	Mean	SD	
MaSF (ours)	0.22	0.03	11.6	0.23	0.93
Mahalanobis [†]	0.54	0.13	28.71	0.39	2.3
GRAM	7.56	0.93	393.64	42.0	31.64

Table 3. Mean of single and total (i.e., time per-sample) statistic execution time (TCT). Relative is $\frac{\text{Total_TCT}}{\text{Network_Time}}$ (12.44 ± 0.32 ms). TCT is averaged over all convolution outputs from MobileNet-V2 with 1K classes. [†]TCT does not include pre-processing (Table-2 results requires an additional backward and forward passes). Network compute and TCT are decoupled, details are available in the Appendix (Section-C).

— by hierarchically combining evidence from the network’s intermediate activations. Schemes based on this framework maintain the false positive rate for unseen datasets and does not rely on prior knowledge regarding the test distribution.

Next, we present a detection scheme dubbed MaSF (Max-Simes-Fisher). MaSF is compared to current OOD detection methods and demonstrates equivalent or better detection power. Our procedure is also more efficient compared to other methods, a crucial property for real-world applications. Moreover, we discuss potential avenues to further reduce the computational overhead via sparsity (i.e., channel sampling) with marginal test power loss.

We believe the proposed framework can be useful for other applications as well. One potential avenue is to statistically test various hypotheses on the CNN itself. For instance, one can detect which channels are significant for the detection

Channels	5%	10%	25%	50%	75%	100%
mTPR	94.4	95.2	95.5	95.8	95.9	96.1
SD	5.5	5.0	4.7	4.6	4.5	4.4
Min-TPR95	76.8	81.8	84.6	85.5	85.9	86.3
*Reduction	x20	x10	x4	x2	x1.33	x1

Table 4. mTPR for MaSF on OOD benchmark-5.1 with random channel selection. MaSF maintains negligible degradation (< 1%) while using only 10% of the total number of channels. Channels are sampled at a fixed rate per layer and results are aggregated over 5 random seeds. *Theoretical cost reduction for MaSF TCT is linear in the number of channels.

of specific classes. This can be used for network analysis or even to reduce inference cost. Other use cases include active or continual learning as a scoring mechanism to detect novel samples. Another example is to use our framework to filter unwanted outlier samples from large unlabeled datasets in self/semi-supervised scenarios.

Better OOD detection schemes can be developed based on our framework, leveraging more sophisticated hierarchical testing methods such as (Benjamini & Bogomolov, 2014; Heller et al., 2018). Incorporating modern combination methods can also help that goal. For example, tests such as (Vovk & Wang, 2020) can deal with dependencies, or tests utilizing random sampling of features (Frostig & Benjamini, 2019).

References

- Abramovich, F. and Ritov, Y. *Statistical theory: a concise introduction*. CRC Press, 2013.
- Bai, Z. and Saranadasa, H. Effect of high dimension: by an example of a two sample problem. *Statistica Sinica*, pp. 311–329, 1996.
- Benjamini, Y. and Bogomolov, M. Selective inference on multiple families of hypotheses. *Journal of the Royal Statistical Society: Series B: Statistical Methodology*, pp. 297–318, 2014.
- Biggio, B., Corona, I., Maiorca, D., Nelson, B., Šrndić, N., Laskov, P., Giacinto, G., and Roli, F. Evasion attacks against machine learning at test time. *Lecture Notes in Computer Science*, pp. 387–402, 2013. ISSN 1611-3349. doi: 10.1007/978-3-642-40994-3_25. URL http://dx.doi.org/10.1007/978-3-642-40994-3_25.
- Blundell, C., Cornebise, J., Kavukcuoglu, K., and Wierstra, D. Weight uncertainty in neural networks, 2015.
- Bridle, J. S. Probabilistic interpretation of feedforward classification network outputs, with relationships to statistical pattern recognition. In *Neurocomputing*, pp. 227–236. Springer, 1990.
- Burda, Y., Edwards, H., Pathak, D., Storkey, A., Darrell, T., and Efros, A. A. Large-scale study of curiosity-driven learning, 2018.
- Cheng, L. and Sheng, X. S. Combination of “combinations of p values”. *Empirical Economics*, 53(1):329–350, 2017.
- Cordella, L. P., De Stefano, C., Tortorella, F., and Vento, M. A method for improving classification reliability of multilayer perceptrons. *IEEE Transactions on Neural Networks*, 6(5):1140–1147, 1995.
- Eykholt, K., Evtimov, I., Fernandes, E., Li, B., Rahmati, A., Xiao, C., Prakash, A., Kohno, T., and Song, D. Robust physical-world attacks on deep learning models, 2017.
- Fisher, R. A. Statistical methods for research workers. In *Breakthroughs in statistics*, pp. 66–70. Springer, 1992.
- Frostig, T. and Benjamini, Y. Testing the equality of multivariate means when $p > n$ by combining the hoteling and simes tests. *arXiv preprint arXiv:1912.10472*, 2019.
- Geifman, Y. and El-Yaniv, R. Selective classification for deep neural networks. In *Advances in neural information processing systems*, pp. 4878–4887, 2017.
- Goodfellow, I. J., Shlens, J., and Szegedy, C. Explaining and harnessing adversarial examples. *arXiv preprint arXiv:1412.6572*, 2014.
- Grosse, K., Manoharan, P., Papernot, N., Backes, M., and McDaniel, P. On the (statistical) detection of adversarial examples, 2017.
- He, K., Zhang, X., Ren, S., and Sun, J. Deep residual learning for image recognition. In *Proceedings of the IEEE conference on computer vision and pattern recognition*, pp. 770–778, 2016.
- Heller, R. and Heller, Y. Multivariate tests of association based on univariate tests. In *Advances in Neural Information Processing Systems*, pp. 208–216, 2016.
- Heller, R., Chatterjee, N., Krieger, A., and Shi, J. Post-selection inference following aggregate level hypothesis testing in large-scale genomic data. *Journal of the American Statistical Association*, 113(524):1770–1783, 2018.
- Hellman, M. The nearest neighbor classification rule with a reject option. *IEEE Trans. Syst. Sci. Cybern.*, 6:179–185, 1970.
- Hendrycks, D. and Gimpel, K. A baseline for detecting misclassified and out-of-distribution examples in neural networks, 2016.
- Hendrycks, D., Mazeika, M., and Dietterich, T. Deep anomaly detection with outlier exposure, 2018.
- Hochberg, Y. A sharper bonferroni procedure for multiple tests of significance. *Biometrika*, 75(4):800–802, 1988.
- Holm, S. A simple sequentially rejective multiple test procedure. *Scandinavian journal of statistics*, pp. 65–70, 1979.
- Hsu, Y.-C., Shen, Y., Jin, H., and Kira, Z. Generalized odin: Detecting out-of-distribution image without learning from out-of-distribution data, 2020.
- Huang, G., Liu, Z., and Weinberger, K. Q. Densely connected convolutional networks. *CoRR*, abs/1608.06993, 2016. URL <http://arxiv.org/abs/1608.06993>.
- Krizhevsky, A. et al. Learning multiple layers of features from tiny images. Technical report, Citeseer, 2009.
- Lee, K., Lee, K., Lee, H., and Shin, J. A simple unified framework for detecting out-of-distribution samples and adversarial attacks, 2018.
- Liang, S., Li, Y., and Srikant, R. Enhancing the reliability of out-of-distribution image detection in neural networks, 2017.
- MacKay, D. A practical bayesian framework for backpropagation networks. *Neural Computation*, 4:448–472, 1992.

- Malinin, A. and Gales, M. Predictive uncertainty estimation via prior networks, 2018.
- Netzer, Y., Wang, T., Coates, A., Bissacco, A., Wu, B., and Ng, A. Y. Reading digits in natural images with unsupervised feature learning. 2011.
- Papadopoulos, H. Inductive conformal prediction: Theory and application to neural networks. In *Tools in artificial intelligence*. Citeseer, 2008.
- Pearson, K. X. on the criterion that a given system of deviations from the probable in the case of a correlated system of variables is such that it can be reasonably supposed to have arisen from random sampling. *The London, Edinburgh, and Dublin Philosophical Magazine and Journal of Science*, 50(302):157–175, 1900.
- Quintanilha, I. M., de ME Filho, R., Lezama, J., Delbracio, M., and Nunes, L. O. Detecting out-of-distribution samples using low-order deep features statistics. 2018.
- Raghuram, J., Chandrasekaran, V., Jha, S., and Banerjee, S. Detecting anomalous inputs to dnn classifiers by joint statistical testing at the layers. *arXiv preprint arXiv:2007.15147*, 2020.
- Sandler, M., Howard, A., Zhu, M., Zhmoginov, A., and Chen, L.-C. Mobilenetv2: Inverted residuals and linear bottlenecks, 2019.
- Sastry, C. S. and Oore, S. Zero-shot out-of-distribution detection with feature correlations. 2019.
- Schölkopf, B., Williamson, R. C., Smola, A. J., Shawe-Taylor, J., and Platt, J. C. Support vector method for novelty detection. In *Advances in neural information processing systems*, pp. 582–588, 2000.
- Simes, R. J. An improved bonferroni procedure for multiple tests of significance. *Biometrika*, 73(3):751–754, 1986.
- Szegedy, C., Zaremba, W., Sutskever, I., Bruna, J., Erhan, D., Goodfellow, I., and Fergus, R. Intriguing properties of neural networks, 2013.
- Vovk, V. and Wang, R. Combining p-values via averaging. *Biometrika*, 107(4):791–808, 2020.
- Winkens, J., Bunel, R., Roy, A. G., Stanforth, R., Natarajan, V., Ledsam, J. R., MacWilliams, P., Kohli, P., Karthikesalingam, A., Kohl, S., Cemgil, T., Eslami, S. M. A., and Ronneberger, O. Contrastive training for improved out-of-distribution detection, 2020.
- Wu, J., Zhang, Q., and Xu, G. Tiny imagenet challenge. Technical report, Technical report, Stanford University, 2017. Available online at [http ...](http://...), 2017.
- Yu, S., Lee, D., and Yu, H. Out-of-distribution image detection using the normalized compression distance, 2020. URL <https://openreview.net/forum?id=H1livgrFvr>.
- Zhang, H., Li, A., Guo, J., and Guo, Y. Hybrid models for open set recognition. *arXiv preprint arXiv:2003.12506*, 2020.
- Zisselman, E. and Tamar, A. Deep residual flow for out of distribution detection, 2020.

A. Notation

B. Statistical procedure details

B.1. Theoretical validity

We are interested in two distinct hypotheses to test. The first one, is to identify if the image is OOD,

$$\mathcal{H}_0^* : \exists c : X_{\text{test}} \sim \mathcal{P}^c, \quad \mathcal{H}_1^* : X_{\text{test}} \not\sim \mathcal{P}^c \quad \forall c \in [k], \quad (7)$$

i.e., the goal is to find if there is a class distribution which the image was sampled from. The hypothesis can be tested using $q^{\max}(X_{\text{test}})$, yielding a valid test (i.e., a test which maintains the significance level, α).

Proof of Proposition 1 We begin by assuming that the true class of X_{test} is y_{test} . Therefore,

$$P_{\mathcal{H}_0^*}(q^{y_{\text{test}}} \leq \alpha) = E(I[q^{y_{\text{test}}} \leq \alpha] | \chi^{y_{\text{test}}}) \leq \alpha. \quad (8)$$

Since, $q^{\max}(X_{\text{test}}) \geq q^{y_{\text{test}}}$ it implies that $P_{\mathcal{H}_0^*}(q^{\max}(X_{\text{test}}) \leq \alpha) \leq \alpha$, concluding the proof. Note, that if the distributions are continuous, the the bound in Eq. 8 is tight.

The second hypothesis of interest is $\mathcal{H}_0^{\hat{y}_{\text{test}}}$,

$$\mathcal{H}_0^{\hat{y}_{\text{test}}} : X_{\text{test}} \sim \mathcal{P}^{\hat{y}_{\text{test}}}, \quad \mathcal{H}_1^{\hat{y}_{\text{test}}} : X_{\text{test}} \not\sim \mathcal{P}^{\hat{y}_{\text{test}}}, \quad (9)$$

In this case, we are interested to know if the image is sampled from the same distribution of the class predicted for it. We now turn to find the required adjustment presented in Proposition 2.

Proof of Proposition 2

$$\begin{aligned} P_{\mathcal{H}_0^{\hat{y}_{\text{test}}}}(q^{\hat{y}_{\text{test}}} \leq \alpha) &= P_{\mathcal{H}_0^{\hat{y}_{\text{test}}}}(q^{\hat{y}_{\text{test}}} \leq \alpha | \hat{y}_{\text{test}} = y_{\text{test}}) \times P(\hat{y}_{\text{test}} = y_{\text{test}}) + \\ &P_{\mathcal{H}_0^{\hat{y}_{\text{test}}}}(q^{\hat{y}_{\text{test}}} \leq \alpha | \hat{y}_{\text{test}} \neq y_{\text{test}}) \times P(\hat{y}_{\text{test}} \neq y_{\text{test}}). \end{aligned}$$

The equality is according to the law of total probability. Since, $P_{\mathcal{H}_0^{\hat{y}_{\text{test}}}}(q^{\hat{y}_{\text{test}}} \leq \alpha | \hat{y}_{\text{test}} \neq y_{\text{test}}) \leq 1$, we obtain,

$$P_{\mathcal{H}_0^{\hat{y}_{\text{test}}}}(q^{\hat{y}_{\text{test}}} \leq \alpha) \leq \alpha \times P(\hat{y}_{\text{test}} = y_{\text{test}}) + 1 \times P(\hat{y}_{\text{test}} \neq y_{\text{test}}).$$

Assuming \hat{y}_{test} is given by the CNN classification, then if the network does not make any mistake, the test is valid. If not, then the significance level needs to be corrected. Since, we already calibrate the significance level in our experiments in order to compare with the various competing methods, we ignore it there.

B.2. Empirical evidence of method validity

This section presents simulation and methods relating to the validity of the suggested framework and MaSF specifically. According to the theory presented above, the resulting p-values from our procedure should follow a uniform (or stochastically larger than uniform) distribution. We graphically assess the resemblance of the distributions using a qq-plot, in which the quantiles of the uniform distribution are plotted vs. the quantiles of the p-values distribution. The identity line will represent a distribution exactly matching the uniform distribution quantiles. Curves below/above it represent stochastically smaller/larger than uniform distributions.

We begin by examining the max p-values when using [Lee et al. \(2018\)](#) benchmark, used to report Table 2 results. The distribution indeed appears uniform or stochastically larger, e.g. the maximum (although there are no theoretical guarantees for it). The exception is ResNet-34 in which, when inspecting quantiles away from the tails, the distribution appear stochastically smaller than uniform.

In order to assess our theoretical guarantees of the framework we abandon [Lee et al. \(2018\)](#) benchmark. We split our data into three sets: 1. DNN training set. 2. MaSF training set. 3. Test set. Set 1 is used solely to train the DNN. Set 2 is used to estimate the eCDFs. Since we estimate eCDF at both the layer and channel levels, we need to split the dataset again.

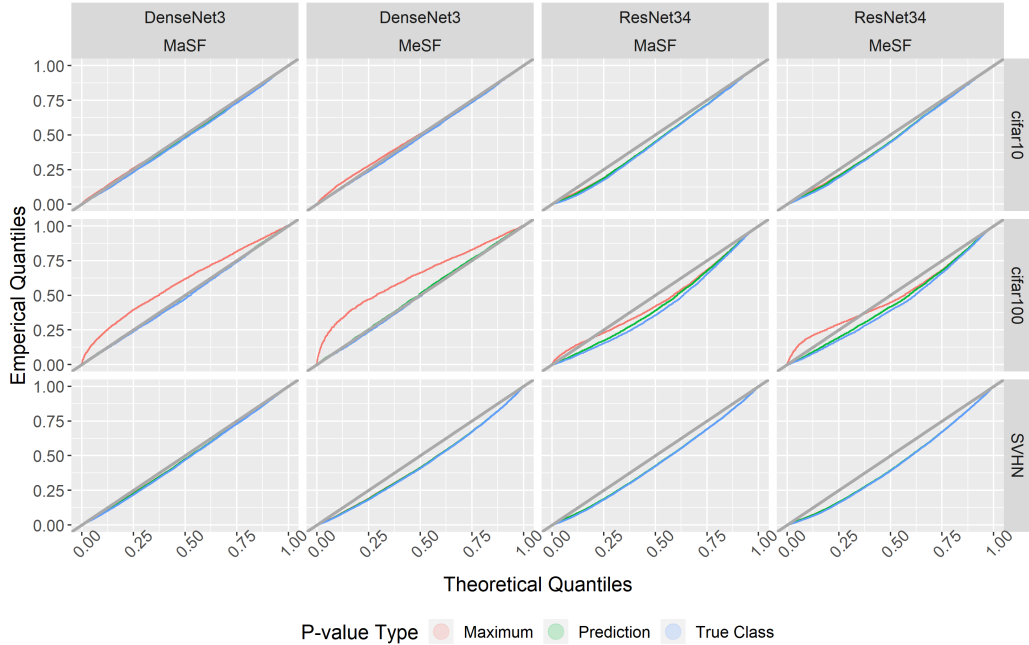


Figure 2. p-values from MaSF and MeSF comparison to uniform [0,1] distribution. eCDFs are estimated using the training data.

Denote the two splits as χ_a^c and χ_b^c , they are used to estimate the eCDF of the channel and layer reductions respectively. If $\chi_a^c \cap \chi_b^c = \emptyset$, the split ensures that the channel eCDF reduction, $\hat{\mathbb{P}}(x; t_{j,l}, \chi_a^c)$, is independent of the layer eCDF reduction $\hat{\mathbb{P}}(x; t^c, \chi_b^c)$. Intuitively, if the p-values at the channel level are obtained from the same data that is used to estimate the channel reduction eCDF, they will tend to be larger than p-value resulting from observations independent of the eCDF. This makes new observations to appear "unusual". By applying the procedure we have an unbiased estimation of the eCDFs, resulting in a valid test. We examine the resulting p-values using this procedure on the test test, and they are assessed using qq-plots (Figs. 2, 3). In our experiments we focused on SVHN and CIFAR-10 (CIFAR-100 has a smaller validation set). We split their validation set as follows (the number of samples is per class): 450 samples for estimating the channels reduction eCDF, 450 samples for estimating the layers reduction eCDF, and 100 samples to estimate the p-values distribution.

Note, the splitting of the training set can be more efficient. Instead of estimating the eCDF on one part and applying it on the other. One can instead, estimate the eCDF of each part, and apply them on observations of the complementary set. This results with more observations being used to estimate the eCDFs (one can combine the eCDFs by averaging for example). Furthermore, the splitting of the data is required since we estimate the eCDFs before hand. If we were to keep a number of observations and estimate the eCDFs together with the test observation (at test time), they are exchangeable, and no splitting is required. This method, depending on the number of observations kept, can be lead to smaller p-values, however, it is much more computationally expensive.

We use the the simulation to demonstrate the theory. The p-values indeed follow a uniform distribution, when splitting the data and ensuring the independence of each step. This implies that for all significance levels our framework yields a valid test.

The subsequent split of the validation set is required in all methods in which the test statistic is a function of estimated distributions. Implying for example, that in order to incorporate the GRAM into our framework, two splits are required (see Section-F.2 for further details).

C. Experimental settings

Models and in-dist datasets. In our experiments we focus on popular vision architectures: DenseNet (Huang et al., 2016) and ResNet-v1 (He et al., 2016). We follow the benchmark proposed by (Lee et al., 2018), reusing the same pretrained models, datasets and evaluation code to report our results. Each architecture (DenseNet-BC & ResNet-34) is paired with a

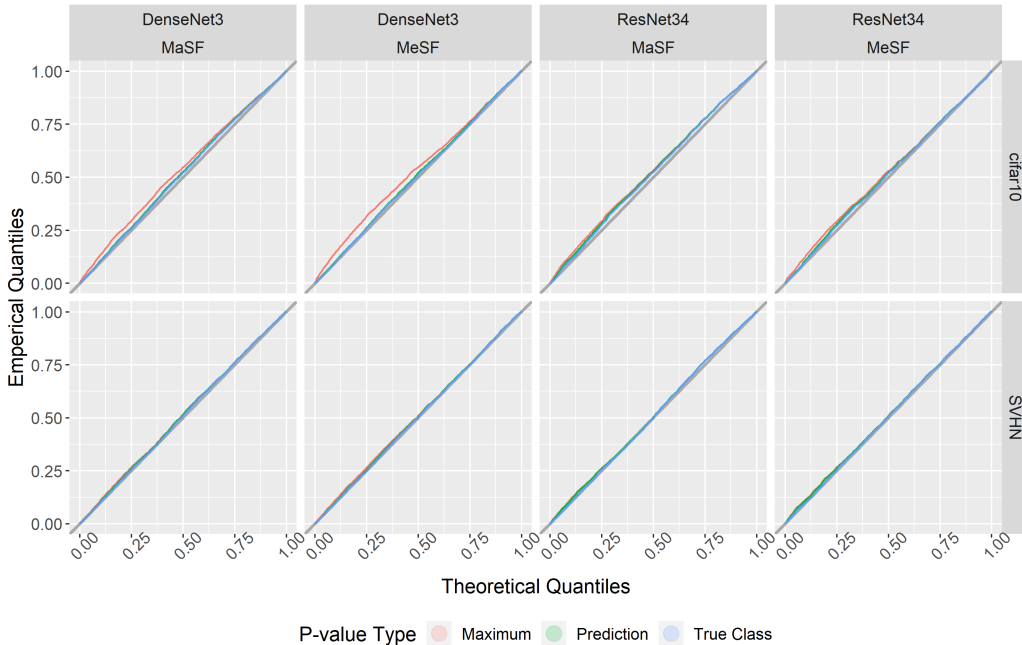


Figure 3. p-values from MaSF and MeSF comparison to uniform [0,1] distribution. eCDFs are estimated on holdout data from the validation set. CIFAR-100 was removed due to the small number of observations.

set of weights, trained on CIFAR-10, CIFAR-100 (Krizhevsky et al., 2009) and SVHN (Netzer et al., 2011). the appropriate training dataset is referred to as the in-distribution while results are reported on the full validation split.

OOD datasets. We evaluate the OOD detection on the resized variants of LSUN (Burda et al., 2018) and Tiny-ImageNet (Wu et al., 2017) as processed and shared by (Liang et al., 2017). We similarly include CIFAR-10 and SVHN validation splits when they are not used for model training.

General calibration settings. Our proposed method requires estimating the statistics’ class conditional distributions (i.e., the empirical CDF) over the calibration set to extract p-values. Thus, we effectively collect a set of percentiles for each statistic and every class in the in-distribution dataset. In our experiments, each sample is used once and without any typical train-time augmentations (i.e., we only apply the required manipulations for inference such as normalization and resize).

Furthermore, since our objective is rejecting \mathcal{H}_0^c or \mathcal{H}_0^* , we can focus on estimating percentiles at the edge of the spectrum for each statistic (i.e., the distribution tails), which improves the sensitivity to abnormal observations. For instance, when performing Simes combination test, the output p-value is scaled proportionally to the number of channels and rank. Therefore, layers with many channels will require an extreme observation in one channel to reflect abnormality for the entire layer (see Appendix-E for more details).

In our experiments, we estimate percentiles between 0.1 and 0.9 at 0.1 increments. In addition we collect smaller than 0.025 and greater than 0.975 for the two-tails test per channel statistics. For the layer combination test we simply use a uniform p-value resolution of $1e-3$. We remind the reader that a high resolution of percentiles is not needed for testing but improves the estimation of the produced p-value distribution, which we use for the empirical validation of the method in Appendix-B.2.

Since any hardware has a limited amount of memory, we cannot always observe the entire calibration data at the same time, for simplicity we average percentiles over fixed size batches. Therefore, the minimal percentile resolution is $\frac{1}{\text{batch size}}$. In our experiments, we use a batch size of 1000 samples of each class for models trained on CIFAR-10 and SVHN. For CIFAR-100, we use a batch-size of 500 due to the limited number of examples per class.

When the calibration set size permits(i.e., there are more samples than can fit in a single batch), we also collect the top and bottom 200 values observed during the entire calibration process to improve tails quantiles estimation. After observing the entire calibration set, we select 10 percentiles at regular intervals from the end of each tail. The resulting percentiles are

determined by the total number of examples in the calibration data.

Test statistic Computation Time. Our measurements for Table-3 include:

- MaSF includes spatial max-pooling operation, followed by a sort operation required by the Simes test. MaSF p-value lookup time is discounted.
- Mahalanobis time includes average-pooling followed by Mahalanobis distance for all classes under LDA assumption. Computation is done in matrix form to optimize execution time. Moreover, it does not include input pre-processing which was used by the original authors to produce results reported in Table2.
- Gram time includes computation of the Gram deviation score over 10 matrix powers.
- Total inference time for MobileNet-V2 with 1K classes and a synthetic input of shape (1,3,224,224).

When calculating the mean of single and total (i.e., time per-sample) statistic execution time (TCT), we measure the wall time over the all convolution layers’ outputs, that are induced using a synthetic input. Global-mTCT times are measured over 10k + 1k warm-up iterations, while statistics are computed sequentially (blocking next layer statistic until current statistic compute is done). Single-mTCT is also averaged over all monitored layers.

Hardware used to produce results is based on 2 x Intel(R) Xeon(R) Gold 6152 CPU @ 2.10GHz system with a 2080ti GPU. Environment is based on Ubuntu 18.04, PyTorch 1.6, cuda 10.2, cudnn 7.6.5. Network compute and TCT are decoupled and do not compete over compute resources.

D. Additional analysis

D.1. Channel reduction statistic distribution

In Fig. 4, we illustrate the distribution of mean and max spatial reductions per-channel in ResNet34 for a single class compared to other classes within the calibration set.

The distributions appears to be uni-modal, while abnormality can be higher or lower than the target class statistic. This supports our choice of a two-tail test for MaSF. Similar assumption can be easily validated for any reduction and data during the design phase of a new method, given knowledge on the in-distribution.

We note that we did not find substantial evidence that favours prioritizing channels based on such inter-class discrimination, compared to a simple random choice in our preliminary OOD detection experiments. However, this is an intriguing avenue for future work.

D.2. Layer correlation analysis

The correlation between p-values of different layers seems to be a property of the network rather than that of a specific data-set or the test statistic used (comparing Fig. 5 A and Fig. 7 B). It can be seen that for both ResNet34 and DenseNet, sequential as well as skip connection layers are strongly correlated and that the correlation tends to intensify as among layers at the end of the network (Fig. 5 - 7). In addition, the correlation does vary greatly for different test statistics (see Fig. 6).

Our method uses the Fisher combination test to combine p-values from layers. Usually, it requires the assumption of independence, however, we have circumvented it by estimating the statistic eCDF (under \mathcal{H}_0). We find that when combining the log p-values the variance of the statistic can be very large due to the strong correlations. Since the power of the test is a function of the overlapping between the distributions under the null and alternative hypotheses, a reasonable strategy is to reduce the variance of the statistics.

A simple method of achieving the goal is to select certain layers. However, this can lead to bias since the signal we care for can be located in the omitted layers. Therefore, we use hierarchical clustering to group together layers with low correlation. Then, at each cluster, we combine the p-values using the Fisher combination test. The final p-value is obtained using a simple Simes test. We found that in our experiments reducing the variance led to marginally improving the results, therefore they are not presented. We leave further study of this topic for future work.

Statistical Testing for Efficient Out of Distribution Detection in Deep Neural Networks

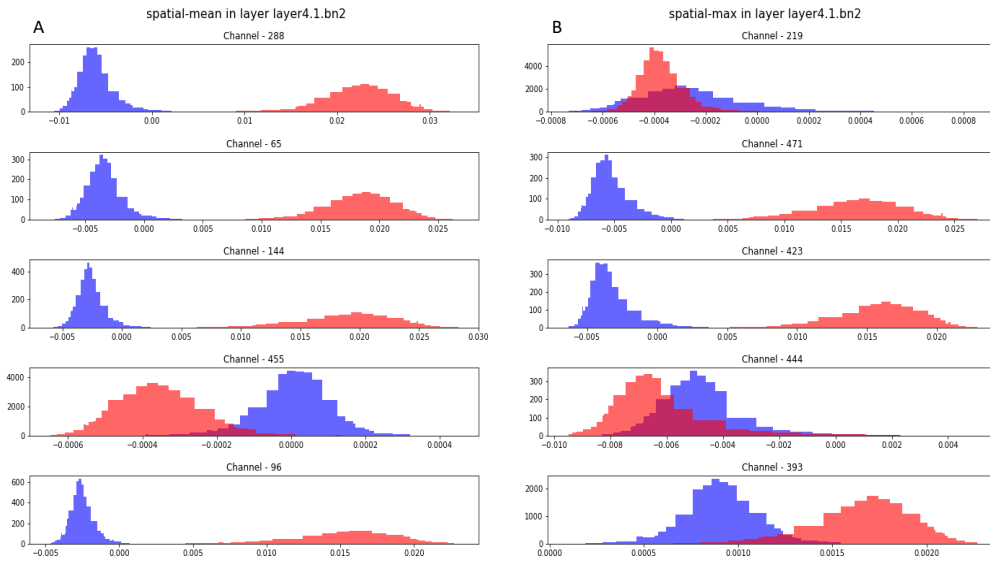


Figure 4. Histogram visualization of max and mean spatial reductions in the ResNet34 for selected layers and channels for two in-distribution classes of CIFAR-10.

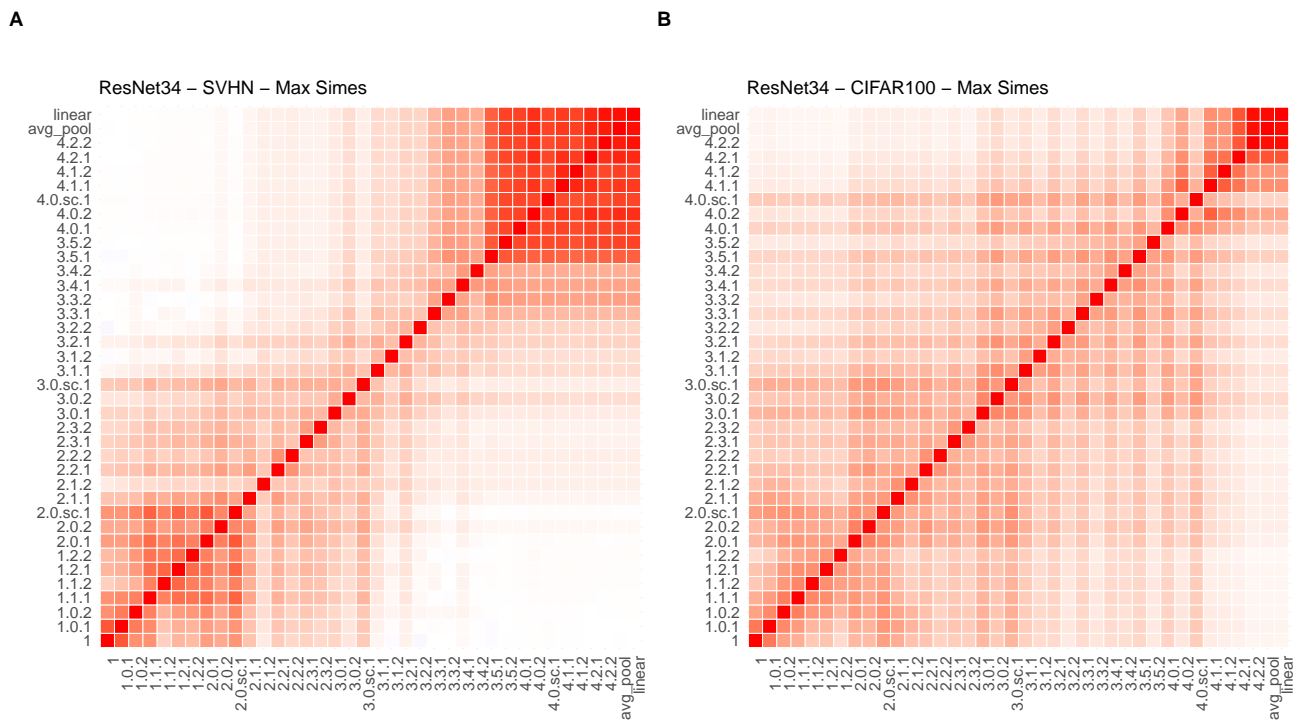


Figure 5. Comparing the correlation of layer level p-values for MaSF, between CIFAR-100 and SVHN with ResNet34.

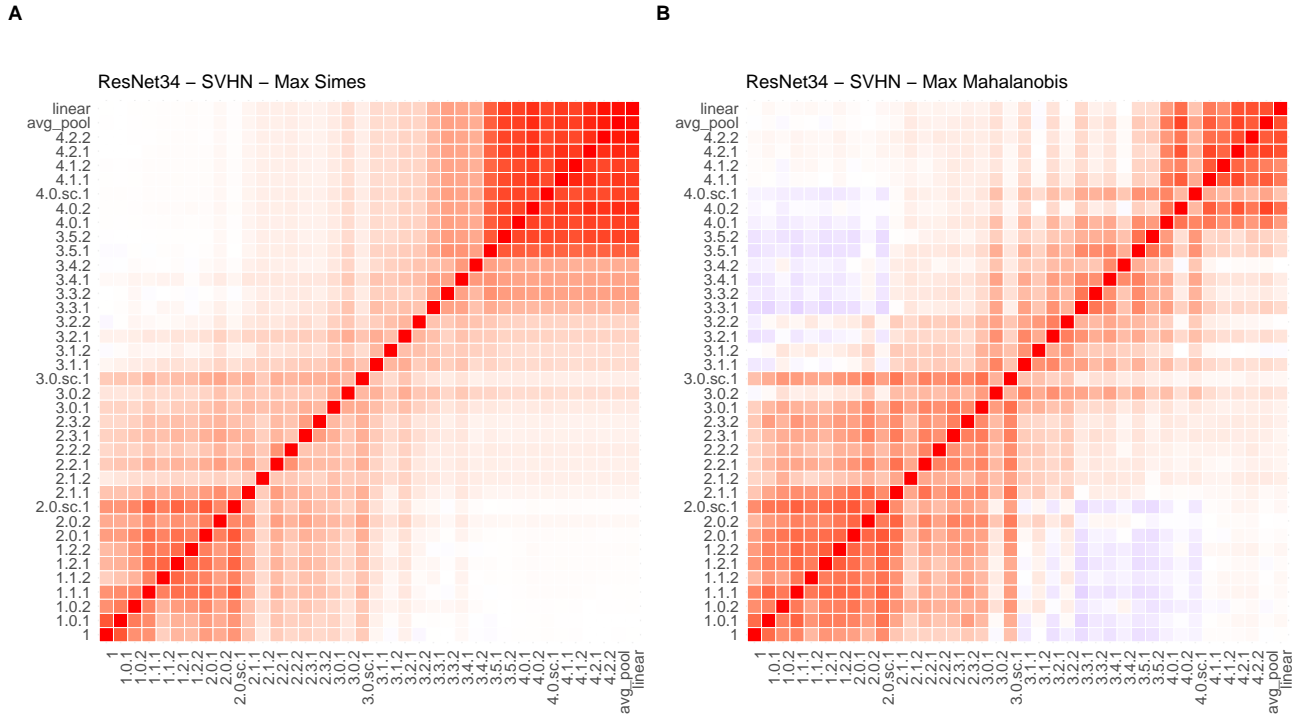


Figure 6. Comparing the MaSF statistic correlation with the MaMF statistic for ResNet34 and SVHN.

E. Testing layers with a large number of channels

We have used the Simes test to combine all channels’ p-values to represent the layer. A possible alternative one may consider, is to simply choose the minimum p-value instead. The issue with this approach is its ignorance of the layer size (i.e., the number of channels). Suppose there are n observations in our calibration set and p channels, assuming the channels are independent, the probability of obtaining the minimal possible p-value, $1/n$, under the null hypothesis, is $(n - 1/n)^p$. As p increase this probability tends to 1, rendering the layer uninformative. Thus, a good combination method should account for the total number of channels.

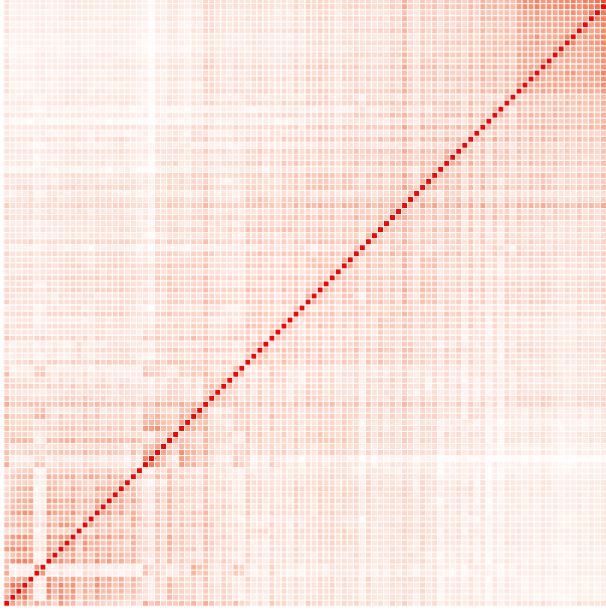
The problem is addressed by the Bonferroni correction, which is a common method for multiple comparisons corrections. It involves multiplying the channels’ p-values by the number of hypotheses considered. Now, we can simply use the corrected minimal p-value. However, for a layer that has more channel than the number of available observations, $n < p$, the obtained p-value will always be 1. This is due to the conservative correction rule. Since, the p-values obtained by the Bonferroni correction, are equal or larger than those from Simes test. The Simes test is uniformly more powerful than the Bonferroni test (Simes, 1986). Other multiple hypotheses correction methods could be applicable such as (Holm, 1979), (Hochberg, 1988) and more.

F. Additional experiments

In this section, we outline our hierarchical testing algorithm. Algorithm-1 describes the generalized approach on which we construct MaSF. in the following sections we will experiment and analyze additional schemes by replacing the spatial and channel reductions.

A

DenseNet3 – CIFAR10 – Max Simes



B

DenseNet3 – SVHN – Max Simes

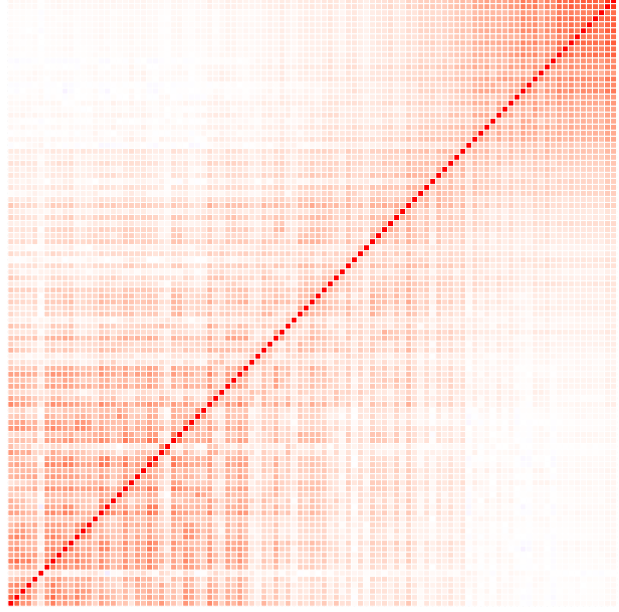


Figure 7. Comparing MaSF statistic on CIFAR100 and SVHN for DenseNet3 model. Layer names are removed for eligibility.

Algorithm 1 Testing an input

```

Input :  $F, \chi^c$ ; // The network, input image and class of interest
Input :  $T^S, T^{\text{ch}}, T^L$ ; // Spatial reduction, channel reduction and layer reduction functions
Input :  $\hat{\mathbb{P}}(\cdot; t_{j,l}^c, \chi^c)$   $j \in [a_l], l \in [L], \hat{\mathbb{P}}^c$ ; // Empirical null distribution of each channel spatial reduction
Input :  $\hat{\mathbb{P}}(\cdot; t^c, \chi^c)$ ; // Empirical null distribution of layer reduction
Output :  $q^c(X_T)$ ; // Class conditional p-value for the input image
for  $l \in [L]$  do
    for  $j \in [a_l]$  do
         $t_{j,l}(X_T) = T^S(F_{j,l}(X_T));$  // Spatial reduction
         $q_{j,l}^c = \min(\hat{\mathbb{P}}(t_{j,l}(X_T); t_{j,l}^c, \chi^c), 1 - \hat{\mathbb{P}}(t_{j,l}(X_T); t_{j,l}^c, \chi^c));$  // P-value of each channel for class  $c$ , assuming
        two sided test
    end
     $t_l^c(X_T) = T^{\text{ch}}(q_{1,l}^c(X_T), \dots, q_{a_l,l}^c(X_T));$  // Applying channel reduction function
end
 $t^c(X_T) = T^L(t_1^c(X_T), \dots, t_L^c(X_T));$  // Applying the layer reduction function
Return  $1 - \hat{\mathbb{P}}(t^c(X_T); t^c, \chi^c);$  // Assuming a right sided p-value
    
```

F.1. Mahalanobis comparison

In Table-5, we present the full results of adapting the Mahalanobis statistics to our framework, dubbed MeMF (Mean-Mahalanobis-Fisher). This is done by computing the Mahalanobis distance over the spatial means for all channel. The resulting distance is converted into a layer p-value using the appropriate eCDF. Finally, the layers are combined using the Fisher test statistic.

Our approach removes the necessity of OOD proxy for calibration, while the resulting detector is guaranteed to maintain TIE. We provide results with and without the LDA assumption (which we refer to as GDA). It can be seen that by utilizing our

Statistical Testing for Efficient Out of Distribution Detection in Deep Neural Networks

Network	In-dist	Out-of-dist	Mahalanobis	MeMF	MeMF (GDA)	MeMF @25%	MeMF @25% (GDA)
DenseNet3	cifar10	SVHN	88.7	90.1	83.1	92.5	88.1
		Imagenet	88.6	94.7	96.6	93.1	95.6
		LSUN	92.4	97.3	98.7	96.6	98.3
	cifar100	SVHN	48.7	65.8	47.6	71.0	60.8
		Imagenet	80.4	89.8	83.0	87.1	86.7
		LSUN	83.8	93.3	84.6	89.9	87.6
	SVHN	cifar10	92.5	78.5	87.1	76.2	80.4
		Imagenet	99.1	99.1	99.6	98.6	99.3
		LSUN	99.7	99.2	99.8	98.8	99.5
ResNet34	cifar10	SVHN	87.5	67.4	64.8	84.1	81.7
		Imagenet	93.1	92.7	93.7	93.6	94.8
		LSUN	99.9	95.9	97.9	97.0	98.3
	cifar100	SVHN	66.5	22.9	0.0	36.0	41.5
		Imagenet	56.7	87.6	0.0	88.4	82.9
		LSUN	38.4	90.1	0.0	89.4	82.8
	SVHN	cifar10	95.2	97.1	98.6	96.0	97.9
		Imagenet	99.3	99.7	99.8	99.7	99.7
		LSUN	99.9	100.0	99.9	99.8	99.9
Average			83.9	86.7	74.2	88.2	87.5
SD			18.8	18.4	35.8	14.8	14.9
Min			38.4	22.9	0.0	36.0	41.5

Table 5. Comparison of the adapted MeMF (Mean-Mahalanobis-Fisher) under LDA and GDA assumptions to Deep Mahalanobis (Lee et al., 2018). GDA suffers from the small number of samples in CIFAR100. Applying random channel selection significantly improves the detector. Deep Mahalanobis results include pre-processing

framework, we improve Mahalanobis detector results (LDA) by 2.82%, although it does not use costly input pre-processing. When LDA assumption is removed (GDA) the Mahalanobis detector severely degrades on CIFAR-100 as expected, due to the small sample size. We also evaluate random channel selection similarly to Section 5.5, results in Table-5 are for the best channel sampling rate. Applying random channel selection significantly improves the detector, specifically in previously failed scenarios.

F.2. GRAM method analysis

The GRAM procedure works well as evident by the results. We wish to understand which elements are essential to its success. To do so we segment the method into 3 components, considering a simple formulation based on a single Gram matrix power.

Spatial reduction. The Gram matrix is effectively used to reduce the spatial dimensions to a single value per-channel via row summation. Then, the min and max parameters are estimated using the observed values per-class. Finally, the statistic can be seen as the per-channel deviation from the estimated extreme parameters. We note that these parameters are essentially quantiles that depend on the total number of examples per class.

Channel reduction. Each layer is summarized using the sum over all per-channel deviations.

Layer reduction. Since the number of channels can impact the scale of each layer deviation. The layer deviation is divided by the expected deviation of the layer ($E_{va}(\delta_l)$), which is measured on 10% of the validation set. This normalizes the contribution of layers with a different number of channels to the total deviation metric. Finally, all normalized deviations are summed together to produce a final abnormality score per sample.

Using the above formulation, we aim to translate these components into similar counterparts within our proposed framework. This allows us to evaluate the importance of each component, which is difficult to perform using the original formulation.

Namely, we split the spatial reduction into 2 separate functions. The first uses only the gram matrix (power-1) reduction denoted as GP_1 , while the second uses either GP_1 or max pooling in conjunction with a modified version of the deviation function (δ^*). Specifically, instead of measuring the maximum and minimum values over the training data, we choose to use

Network	In-dist	Out-of-dist	TPR at 95%			
			GP ₁	GP ₁ + δ^*	Max+ δ^*	
DenseNet	CIFAR-10	SVHN	0.2	95.32	94.69	
		TinyImageNet	78.06	91.54	97.5	
		LSUN	83.3	95.94	99.03	
	CIFAR-100	SVHN	0.58	85.38	81.33	
		TinyImageNet	76.97	85.69	94.22	
		LSUN	81.72	87.02	97.04	
	SVHN	CIFAR-10	43.46	72.57	79.63	
		TinyImageNet	67.07	97.69	99.31	
		LSUN	68.98	97.94	99.58	
	ResNet	CIFAR-10	SVHN	0.29	97.9	93.47
			TinyImageNet	64.3	94.77	98
			LSUN	67.91	98.64	99.3
CIFAR-100		SVHN	0.94	50.92	57.02	
		TinyImageNet	77.26	81.81	94.55	
		LSUN	81.76	79.96	97.03	
SVHN		CIFAR-10	53.23	95.78	82.15	
		TinyImageNet	68.63	99.61	94.24	
		LSUN	68.85	99.61	92.41	
Average			54.64	89.34	91.69	
SD			31.37	12.38	10.69	
Min			0.20	50.92	57.02	

Table 6. Evaluating the importance of key components from GRAM method within our proposed framework. Replacing the Gram matrix with simple max pooling slightly improves OOD detection results. This indicates that the deviation function is more important than the Gram matrix which is the compute intensive part of the method.

less extreme quantiles (0.05 and 0.95). The new deviation function is defined as follows,

$$\delta^*(\text{quantile}_{0.05}, \text{quantile}_{0.95}, \text{value}) = \begin{cases} 0 & \text{quantile}_{0.05} \leq \text{value} \leq \text{quantile}_{0.95} \\ \frac{\text{quantile}_{0.05} - \text{value}}{|\text{quantile}_{0.05}|} & \text{value} < \text{quantile}_{0.05} \\ \frac{\text{value} - \text{quantile}_{0.95}}{|\text{quantile}_{0.95}|} & \text{value} > \text{quantile}_{0.95} \end{cases} \quad (10)$$

The channel reduction remains unchanged, i.e. channels are reduced using a simple summation over the observed values.

For the layer reduction is replaced with the fisher statistic which is better suited for the task of exposing irregularities over all layers compared to simple summation. This also allows us to avoid using $E_{va}(\delta_l)$ normalization, by converting the observed layer deviations with their representing p-value. This leads to a uniform scale across all layers deviations.

We compare these variants on OOD detection tasks, where the main objective is to identify which elements are more dominant in their importance to the detection performance. From Table-6, we observe that δ^* is crucial for OOD detection. We attribute its importance to normalizing the channels according to their magnitudes before adding them to the layer deviation score. On the other hand, when replacing the Gram matrix with a simple max-pooling, the detector is marginally better on average. Based on our evaluation, we posit that the success of the GRAM method could potentially be based more on its deviation function than the specific use of Gram matrix countering the original intuition linked to style transfer. However, it is interesting to see GP_1 clearly outperforms max pooling in certain cases and vice versa.

F.3. Full results

We provide the results from Table-2 including AUROC in Table-7.

Network	In-dist	Out-of-dist	TPR at 95%				AUCROC			
			Mahalanobis	GRAM	Resflow	MaSF	Mahalanobis	GRAM	Resflow	MaSF
DenseNet	CIFAR-10	SVHN	88.7	96.1	86.1	98.5	97.6	99.1	97.3	99.5
		TinyImageNet	88.6	98.8	96.1	97.6	97.5	99.7	99.1	99.1
		LSUN	92.4	99.5	98.1	99	98.3	99.9	99.5	99.4
	CIFAR-100	SVHN	48.7	89.3	48.9	88.9	85.6	97.3	87.9	96.7
		TinyImageNet	80.4	95.7	91.5	93.4	92.7	99	98.1	98.1
		LSUN	83.8	97.2	95.8	96.5	95	99.3	98.9	98.6
	SVHN	CIFAR-10	92.5	80.4	90	88.1	96.7	95.5	98	97.4
		TinyImageNet	99.1	99.1	99.9	99.8	99.5	99.7	99.9	99.5
		LSUN	99.7	99.5	100	100	99.8	99.8	99.9	99.5
ResNet	CIFAR-10	SVHN	87.5	97.6	91	98.9	97.4	99.5	98.2	99.1
		TinyImageNet	93.1	98.7	98	98	97.9	99.7	99.6	98.9
		LSUN	99.9	99.6	99.1	99.5	99.2	99.9	99.8	99.2
	CIFAR-100	SVHN	66.5	80.8	74.1	86.3	93.2	96	95.1	95.6
		TinyImageNet	56.7	94.8	77.5	92.6	76.9	98.9	90.1	97.3
		LSUN	38.4	96.6	70.4	94.4	66.2	99.2	87.2	97.7
	SVHN	CIFAR-10	95.2	85.8	96.6	97.9	98.1	97.3	99	99.1
		TinyImageNet	99.3	99.3	99.9	99.9	99.4	99.7	99.9	99.5
		LSUN	99.9	99.6	100	100	99.9	99.8	100	99.5
Average			83.9	94.9	89.6	96.1	93.9	98.9	97.1	98.5
SD			18.8	6.4	13.8	4.4	9	1.4	4.2	1.2
Minimum			38.4	80.4	48.9	86.3	66.2	95.5	87.2	95.6

Table 7. Full Table-2, including AUROC